

Computing the logarithmic capacity of compact sets having (infinitely) many components with the Charge Simulation Method

Jörg Liesen[†]Mohamed M.S. Nasser[‡]Olivier Sète[§]

March 1, 2023

Abstract

We apply the Charge Simulation Method (CSM) in order to compute the logarithmic capacity of compact sets consisting of (infinitely) many “small” components. This application allows to use just a single charge point for each component. The resulting method therefore is significantly more efficient than methods based on discretizations of the boundaries (for example, our own method presented in [14]), while maintaining a very high level of accuracy. We study properties of the linear algebraic systems that arise in the CSM, and show how these systems can be solved efficiently using preconditioned iterative methods, where the matrix-vector products are computed using the Fast Multipole Method. We illustrate the use of the method on generalized Cantor sets and the Cantor dust.

Keywords. Logarithmic capacity, Charge Simulation Method, Cantor set, Cantor dust, Fast Multipole Method, GMRES method.

AMS. 65E05, 30C85, 31A15, 65F10

1 Introduction

As pointed out by Ransford and Rostand, the computation of the logarithmic capacity of compact subsets of the complex plane is in general a “notoriously hard” problem [24, p. 1499]. This is particularly true for non-connected sets consisting of many, or even infinitely many components. An important and frequently studied example in this context is given by the classical Cantor middle third set and its generalizations, for which no analytic formula for their logarithmic capacity is known. Among the different approaches to computing the logarithmic capacity of these fractal sets are the method of Ransford and Rostand which uses linear programming [24], a method of Banjai, Embree and Trefethen based on Schwarz-Christoffel mappings (also see [24]), the study of the spectral theory of orthogonal polynomials by Krüger and Simon [13], and our algorithm based on conformal maps onto lemniscatic domains [14]. Further numerical methods for computing the logarithmic capacity of compact sets can be found, for example, in [4, 5, 23, 25].

In this paper we derive and study an alternative method for numerically approximating the logarithmic capacity of compact sets consisting of very many “small” components, which uses the *Charge Simulation Method* (CSM) [1, 2, 20], also known as the *Method of*

[†]Institute of Mathematics, Technische Universität Berlin, Straße des 17. Juni 136, 10623 Berlin, Germany. liesen@math.tu-berlin.de, ORCID: 0000-0002-3677-373X

[‡]Department of Mathematics, Statistics, and Physics, Wichita State University, Wichita, KS 67260-0033, USA. mms.nasser@wichita.edu, ORCID: 0000-0002-2561-0978

[§]Institute of Mathematics and Computer Science, Universität Greifswald, Walther-Rathenau-Straße 47, 17489 Greifswald, Germany. olivier.sete@uni-greifswald.de, ORCID: 0000-0003-3107-3053

Fundamental Solutions [3, 30]. In the CSM, the Green's function of the complement of the given compact set is approximated by a linear combination of logarithmic potentials which depend on so-called charge points inside each component of the set. Solving the (dense) linear algebraic system for the coefficients of the linear combination then yields the desired approximation of the logarithmic capacity.

For the types of sets we consider, choosing one charge point in each component is sufficient. A similar approach has been used in [12], where the CSM was used to solve the harmonic image inpainting problem. The linear algebraic system that needs to be solved therefore is significantly smaller than in methods that are based on discretizing the boundaries of each component (for example, our own Boundary Integral Equation (BIE) method presented in [14]). We solve the linear algebraic systems arising in the CSM iteratively with the GMRES method [26]. In order to speed up the iteration we use the centrosymmetric structure of the system matrices, the Fast Multipole Method [9] for computing matrix-vector products, and a problem-adapted preconditioner. We apply the new method to generalized Cantor sets and the Cantor dust. These sets consist of infinitely many components, and we compute approximations of their logarithmic capacities by extrapolating from computed logarithmic capacities of finite approximations that consist of many components. Timing comparisons with our method from [14] show the computational efficiency, and comparisons of the computed capacity values with other published results demonstrate the high accuracy of the new method.

The paper is organized as follows. In Section 2 we present the necessary background on the logarithmic capacity and the CSM. In Section 3 we study the approximation of the logarithmic capacity for generalized Cantor sets, and in Section 4 we do the same for the Cantor dust. The paper ends with concluding remarks in Section 5.

2 Logarithmic capacity and the CSM

Let $E \subseteq \mathbb{C}$ be a compact set and denote $E^c := (\mathbb{C} \cup \{\infty\}) \setminus E$. Suppose that the unbounded connected component G of E^c is regular in the sense that it possesses a *Green's function* $g = g_E = g_G$. Then the *logarithmic capacity* of E , denoted by $\text{cap}(E)$, satisfies

$$\text{cap}(E) = \lim_{z \rightarrow \infty} \exp(\log|z| - g(z)); \quad (1)$$

see, e.g., [22, Theorem 5.2.1], [14, Eq. (2.2)], or Szegő's original article [28]. Recall that the Green's function with pole at infinity of G is the real-valued function such that

1. g is harmonic in $G \setminus \{\infty\}$ and $g(z) - \log|z|$ is bounded in a neighborhood of infinity,
2. g is continuous in $\overline{G} \setminus \{\infty\}$ and vanishes on ∂G .

We assume that the boundary of the unbounded domain G with $\infty \in G$ consists of a finite number of Jordan curves, in which case the Green's function g with pole at infinity of G exists [7, p. 41].

In the CSM, a harmonic function is approximated by a linear combination of fundamental solutions of the Laplace equation, which are logarithmic potentials in the two-dimensional case [3, 30]. In our setting, the Green's function g is approximated by a function of the form

$$h(z) = c + \sum_{j=1}^N p_j \log|z - w_j|, \quad z \in G, \quad (2)$$

where c, p_1, \dots, p_N are undetermined real constants, and where $w_1, \dots, w_N \in \mathbb{C} \setminus \overline{G}$ are pairwise distinct. The points w_1, \dots, w_N are called the *charge points*, and the coefficients

p_1, \dots, p_N the charges [1]. The function h in (2) is harmonic in $\mathbb{C} \setminus \{w_1, \dots, w_N\}$. Since g behaves as $\log|z|$ for $z \rightarrow \infty$, we require

$$\sum_{j=1}^N p_j = 1. \quad (3)$$

The coefficients c, p_1, \dots, p_N in (2) are usually determined from the boundary condition $g(z) = 0$ on ∂G , by imposing the condition $h(z) = 0$ in a finite set of collocation points on ∂G ; see, e.g., [1, 2, 3, 20, 30]. The number of collocation points is usually at least $N + 1$, so that this procedure leads to a square or overdetermined linear algebraic system [30, p. 12]. Below we will use a slightly different approach to obtain a linear algebraic system for the coefficients.

In view of (1), the approximation h of g yields

$$\text{cap}(E) = \lim_{z \rightarrow \infty} \exp(\log|z| - g(z)) \approx \lim_{z \rightarrow \infty} \exp(\log|z| - h(z)) = e^{-c}. \quad (4)$$

The following result gives an error bound for this approximation.

Lemma 2.1. *Let $E \subseteq \mathbb{C}$ be compact such that the unbounded connected component G of E^c is bounded by m Jordan curves, and let g be the Green's function with pole at infinity of G . Let h be as in (2) with (3), then*

$$|\text{cap}(E) - e^{-c}| \leq e^{-c} \left(M + \frac{1}{2} M^2 e^M \right), \quad (5)$$

where $M := |\hat{c} - c| \leq \max_{\zeta \in \partial G} |h(\zeta)|$ and $\hat{c} := \lim_{z \rightarrow \infty} (g(z) - \log|z|) \in \mathbb{R}$.

Proof. As above, let $w_1 \in \mathbb{C} \setminus \overline{G}$ be the first charge point. The auxiliary functions

$$u(z) = g(z) - \log|z - w_1|, \quad v(z) = h(z) - \log|z - w_1|,$$

are continuous in \overline{G} and harmonic in G , including at infinity with $u(\infty) = \hat{c}$ and $v(\infty) = c$. Since $w_1 \notin \overline{G}$, the Möbius transformation $\varphi(z) = 1/(z - w_1)$ maps G onto the bounded domain $R = \varphi(G)$, whose boundary consists of m Jordan curves. The functions $u \circ \varphi^{-1}$ and $v \circ \varphi^{-1}$ are harmonic in R and continuous in \overline{R} . Then, by the maximum principle for harmonic functions on bounded domains (see, e.g., [22, Theorem 1.1.8]),

$$|(u \circ \varphi^{-1})(w) - (v \circ \varphi^{-1})(w)| \leq \max_{\omega \in \partial R} |(u \circ \varphi^{-1})(\omega) - (v \circ \varphi^{-1})(\omega)|, \quad w \in \overline{R}.$$

This yields

$$|u(z) - v(z)| \leq \max_{\zeta \in \partial G} |u(\zeta) - v(\zeta)| = \max_{\zeta \in \partial G} |g(\zeta) - h(\zeta)| = \max_{\zeta \in \partial G} |h(\zeta)|, \quad z \in \overline{G}.$$

The last equality holds since g vanishes on ∂G . Taking the limit $z \rightarrow \infty$ we obtain $|\hat{c} - c| \leq \max_{\zeta \in \partial G} |h(\zeta)|$. The estimate (5) follows from $\text{cap}(E) = e^{-\hat{c}}$ and Taylor's formula. \square

On the right hand side of (5) we can replace the (in general unknown) quantity M by the upper bound given by the maximum of the (known) function h on ∂G . In this way we obtain a computable upper bound on the error. We will give an example in Section 3.2.

Remark 2.2. We give another interpretation of the approximation $e^{-c} \approx \text{cap}(E)$ in the case $p_1, \dots, p_N > 0$. Then $h(z) > 0$ is equivalent to $\prod_{j=1}^N |z - w_j|^{p_j} > e^{-c}$. Since the real numbers $p_1, \dots, p_N > 0$ are not necessarily rational, the set $\mathcal{L} = \{z \in \mathbb{C} \cup \{\infty\} : h(z) > 0\}$ is the exterior of a generalized lemniscate. This is an unbounded domain (with $\infty \in \mathcal{L}$), and h is the Green's function with pole at infinity of \mathcal{L} . In particular, e^{-c} is the logarithmic capacity of the compact set \mathcal{L}^c . If \mathcal{L} has connectivity N , it is a *lemniscatic domain*;

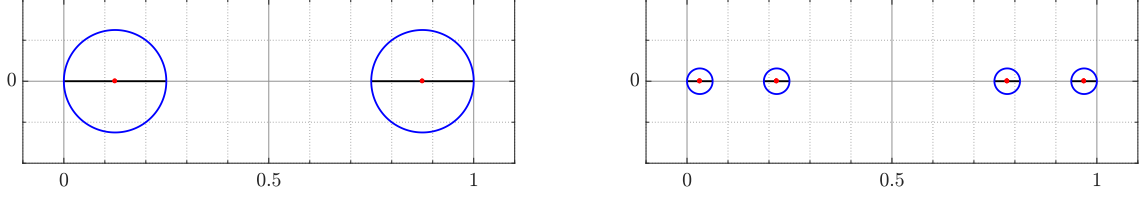


Figure 1: The sets E_1, D_1 (left) and E_2, D_2 (right) for $q = 1/4$.

see [27, 18] and references therein as well as Walsh's original article [29]. Otherwise, the connectivity of \mathcal{L} is lower, and \mathcal{L} is the exterior of a level curve of the Green's function of a lemniscatic domain. Thus, in the method we propose here, the original domain $G = E^c$ is approximated by the domain \mathcal{L} , and the method returns $\text{cap}(\mathcal{L}^c)$ as approximation of $\text{cap}(G^c) = \text{cap}(E)$.

If not all charges are positive, then the set $\{z \in \mathbb{C} \cup \{\infty\} : h(z) > 0\}$ is a canonical domain of the more general form in [29, Theorem 3].

In the following two sections, we will apply the CSM in order to compute (approximations of) the logarithmic capacity of generalized Cantor sets (Section 3) and the Cantor dust (Section 4).

3 Generalized Cantor sets

In this section, we start with setting up the CSM for the generalized Cantor sets. Next, we give an analytic example (illustrating this approach and Lemma 2.1), and study the structure and properties of the matrices arising in the CSM. We then show how the resulting linear algebraic systems can be solved iteratively, and finally we present the results of numerical computations of the logarithmic capacity of generalized Cantor sets.

3.1 Setting up the CSM

Fix some $q \in (0, 1/2)$, let $E_0 := [0, 1]$, and define recursively

$$E_k := qE_{k-1} \cup (qE_{k-1} + 1 - q), \quad k \geq 1. \quad (6)$$

Thus, the set E_k is obtained by removing the middle $1 - 2q$ from each interval of the set E_{k-1} ; see Figure 1 for E_1 (left) and E_2 (right) corresponding to $q = 1/4$. Then the generalized Cantor set $E = E(q)$ is defined as

$$E := \bigcap_{k=0}^{\infty} E_k. \quad (7)$$

For $q = 1/3$ we obtain the classical Cantor middle third set. The limiting cases are $E = \{0, 1\}$ for $q = 0$ and $E = [0, 1]$ for $q = 1/2$.

The set E_k consists of $m = 2^k$ disjoint intervals $I_{k,j}$, $j = 1, 2, \dots, m$, numbered from left to right. The intervals have same length

$$|I_{k,1}| = |I_{k,2}| = \dots = |I_{k,m}| = q^k. \quad (8)$$

Denote the midpoint of $I_{k,j}$ by $w_{k,j}$. Let

$$r_k = \frac{1}{2}q^k = w_{k,1}, \quad (9)$$

then

$$0 < r_k = w_{k,1} < w_{k,2} < \dots < w_{k,m} = 1 - r_k < 1. \quad (10)$$

Instead of the sets E_k consisting of closed intervals we will use sets D_k consisting of closed disks in the CSM. More precisely, let

$$D_0 := \left\{ z \in \mathbb{C} : \left| z - \frac{1}{2} \right| \leq \frac{1}{2} \right\},$$

and define recursively

$$D_k := qD_{k-1} \cup (qD_{k-1} + 1 - q), \quad k \geq 1.$$

Then D_k consists of $m = 2^k$ disjoint disks $D_{k,j}$ with the centers $w_{k,j}$, $j = 1, 2, \dots, m$, i.e.,

$$D_k = \bigcup_{j=1}^m D_{k,j};$$

see Figure 1 for D_1 (left) and D_2 (right) corresponding to $q = 1/4$. All of the m disks have the same radius r_k from (9). Since $E_0 = D_0 \cap \mathbb{R}$, we obtain $E_k = D_k \cap \mathbb{R}$ for all $k \geq 1$ by induction. Moreover, we have the following result.

Theorem 3.1. *In the notation established above,*

$$\bigcap_{k=0}^{\infty} D_k = E \quad \text{and} \quad \text{cap}(E) = \lim_{k \rightarrow \infty} \text{cap}(D_k).$$

Proof. Clearly, $E \subseteq D := \bigcap_{k=0}^{\infty} D_k$. Next, we show that if $z \in \mathbb{C} \setminus E$, then $z \notin D$. If $z \in \mathbb{R} \setminus E$, then there exists $k \in \mathbb{N}$ such that $z \notin E_k = D_k \cap \mathbb{R} \supseteq D \cap \mathbb{R}$, hence $z \notin D$. If $z \in \mathbb{C} \setminus \mathbb{R}$, i.e., $|\text{Im}(z)| > 0$, then there exists $k \in \mathbb{N}$ such that $0 < r_k < |\text{Im}(z)|$, which shows that $z \notin D_k \supseteq D$. Together we obtain $D = E$. Finally, $\text{cap}(E) = \lim_{k \rightarrow \infty} \text{cap}(D_k)$ by [22, Theorem 5.1.3], since $D_0 \supseteq D_1 \supseteq D_2 \supseteq \dots$ are compact and $E = \bigcap_{k=0}^{\infty} D_k$. \square

Our overall strategy for computing an approximation of $\text{cap}(E)$, where the set E consists of infinitely many components, is to first approximate $\text{cap}(D_k)$ for reasonably many and large values of k with the CSM. Then we extrapolate from the computed approximations of $\text{cap}(D_k)$ to obtain an approximation of $\lim_{k \rightarrow \infty} \text{cap}(D_k) = \text{cap}(E)$.

The set $G_k := D_k^c = (\mathbb{C} \cup \{\infty\}) \setminus D_k$ is an unbounded multiply connected domain of connectivity m with

$$\partial G_k = C_{k,1} \cup \dots \cup C_{k,m},$$

where $C_{k,j} := \partial D_{k,j}$ is the circle with center $w_{k,j}$ and radius r_k for $j = 1, 2, \dots, m$.

As described in Section 2, we approximate g_k , the Green's function with pole at infinity of G_k , with the CSM by

$$h_k(z) = c_k + \sum_{\ell=1}^m p_{k,\ell} \log|z - w_{k,\ell}|, \quad z \in G_k, \quad (11)$$

with

$$\sum_{\ell=1}^m p_{k,\ell} = 1. \quad (12)$$

In the CSM for unbounded multiply connected domains, we usually choose many charge points inside each boundary component $C_{k,j}$, $j = 1, 2, \dots, m$ [2, 20]. However, because r_k is very small for large $m = 2^k$, we choose only one point inside $C_{k,j}$, which is its center $w_{k,j}$.

Remark 3.2. The fact that we use just a *single charge point for each boundary component* $C_{k,j}$ is an essential difference to other discretization-based methods for computing the logarithmic capacity of sets consisting of many components. For example, our own BIE method presented in [14] “opens up” the intervals of E_k to obtain a compact set of the

same capacity, but bounded by smooth Jordan curves. The computation of the logarithmic capacity then is based on discretizing the $m = 2^k$ boundary curves using n points on each of them. Consequently, for the same k the linear algebraic systems in the method presented here are smaller by a factor of n compared to those in [14]. This is one of the main reasons for the very significant computational savings that we obtain with the new method; see Section 3.5. Using only a single charge point for each boundary component can be justified by the fact that the boundary components become very small when k increases. This is illustrated in [12] where, as mentioned in the Introduction, a similar approach has been used. (In terms of the current paper, the derivation of the system matrix in [12] assumes that the value of r_k in the equation (14) is negligible in comparison with $|w_{k,j} - w_{k,\ell}|$ for $j \neq \ell$.)

The Green's function g_k of G_k vanishes on the boundary ∂G_k . This does not hold for the approximation h_k . Instead, we require that h_k has zero mean on each circle $C_{k,j}$, i.e.,

$$\frac{1}{2\pi i} \int_0^{2\pi} h_k(\eta_{k,j}(t)) dt = 0, \quad j = 1, \dots, m, \quad (13)$$

with the parametrization $\eta_{k,j}(t) = w_{k,j} + r_k e^{it}$, $0 \leq t \leq 2\pi$. On the circle $C_{k,j}$,

$$\begin{aligned} h_k(\eta_{k,j}(t)) &= c_k + \sum_{\ell=1}^m p_{k,\ell} \log |w_{k,j} + r_k e^{it} - w_{k,\ell}|, \\ &= c_k + p_{k,j} \log r_k + \sum_{\substack{\ell=1 \\ \ell \neq j}}^m p_{k,\ell} \log |w_{k,j} + r_k e^{it} - w_{k,\ell}|, \quad j = 1, \dots, m, \end{aligned} \quad (14)$$

for all $t \in [0, 2\pi]$. For $\ell \neq j$, the function $\log |z - w_{k,\ell}|$ is harmonic in the disk $D_{k,j} = \{z \in \mathbb{C} : |z - w_{k,j}| \leq r_k\}$, hence

$$\frac{1}{2\pi} \int_0^{2\pi} \log |w_{k,j} + r_k e^{it} - w_{k,\ell}| dt = \log |w_{k,j} - w_{k,\ell}|$$

by the mean value property of harmonic functions; see, e.g., [31, Theorem 4.6.7] or [22, Theorem 1.1.6]. Thus, integrating (14) and requiring (13) yields the linear algebraic system

$$c_k + p_{k,j} \log r_k + \sum_{\substack{\ell=1 \\ \ell \neq j}}^m p_{k,\ell} \log |w_{k,j} - w_{k,\ell}| = 0, \quad j = 1, 2, \dots, m. \quad (15)$$

We will now consider (15) for a fixed size $m = 2^k$, and therefore we will drop the index k in the following for simplicity. We write (15) in the form

$$A\mathbf{p} = c\mathbf{e}, \quad (16)$$

where $\mathbf{p} = [p_1, \dots, p_m]^T$, $\mathbf{e} = [1, \dots, 1]^T \in \mathbb{R}^m$, and

$$A = - \begin{bmatrix} \log r & \log |w_1 - w_2| & \cdots & \log |w_1 - w_{m-1}| & \log |w_1 - w_m| \\ \log |w_2 - w_1| & \log r & \cdots & \log |w_2 - w_{m-1}| & \log |w_2 - w_m| \\ \vdots & \vdots & \ddots & \vdots & \vdots \\ \log |w_{m-1} - w_1| & \log |w_{m-1} - w_2| & \cdots & \log r & \log |w_{m-1} - w_m| \\ \log |w_m - w_1| & \log |w_m - w_2| & \cdots & \log |w_m - w_{m-1}| & \log r \end{bmatrix}. \quad (17)$$

Note that $A \in \mathbb{R}^{m,m}$ and that $m = 2^k$ is even.

Theorem 3.3. *For $k \geq 1$, the entries a_{ij} of A satisfy*

$$\log \frac{1}{1-2r} \leq a_{ij} \leq \log \frac{1}{r}, \quad 1 \leq i, j \leq m, \quad (18)$$

and they decay away from the diagonal in each row and column, i.e.,

$$a_{i,1} < \dots < a_{i,i-1} < a_{i,i}, \quad a_{i,i} > a_{i,i+1} > \dots > a_{i,m}, \quad (19)$$

$$a_{1,j} < \dots < a_{j-1,j} < a_{j,j}, \quad a_{j,j} > a_{j+1,j} > \dots > a_{m,j}, \quad (20)$$

for $1 \leq i, j \leq m$.

Proof. Since $0 < r = w_1 < w_2 < \dots < w_m$, we have that

$$|w_i - w_1| > |w_i - w_2| > \dots > |w_i - w_{i-1}| > r, \quad r < |w_i - w_{i+1}| < \dots < |w_i - w_m|,$$

which is equivalent to (19). Since A is symmetric, (19) is equivalent to (20).

Let $1 \leq i, j \leq m$. The upper bound in (18) follows from $a_{ij} \leq a_{ii} = \log(1/r)$. For the lower bound, notice that $|w_i - w_j| \leq 1 - 2r$ by (10), and that $1 - 2r > 0$ if and only if $k \geq 1$. We then obtain $a_{ij} \geq \log \frac{1}{1-2r}$ for $i \neq j$, which also holds for a_{ii} , since a_{ii} is the largest element in the row. \square

We will continue under the assumption that A is nonsingular, which will be justified below; see Section 3.3 as well as Figure 3 and the corresponding discussion. Note that (12) can be written as $\mathbf{e}^T \mathbf{p} = 1$, and therefore multiplying (16) from the left with $\mathbf{e}^T A^{-1}$ yields $1 = \mathbf{e}^T \mathbf{p} = c \mathbf{e}^T A^{-1} \mathbf{e}$ or, equivalently,

$$c = \frac{1}{\mathbf{e}^T A^{-1} \mathbf{e}}. \quad (21)$$

Thus, in order to compute e^{-c} , which is our approximation of $\text{cap}(E)$ (see (4)), we need to compute (or accurately estimate) the quantity $\mathbf{e}^T A^{-1} \mathbf{e}$, preferably without explicitly inverting the full matrix A . One option is to numerically solve the linear algebraic system

$$A\mathbf{x} = \mathbf{e}, \quad (22)$$

and then to compute $c = 1/(\mathbf{e}^T \mathbf{x})$.

3.2 An analytic example: Two disks

In this section, we study the accuracy of the CSM approximation and the tightness of the bounds in Lemma 2.1 on a simple example where an exact formula for the logarithmic capacity is known. We consider the set D_1 consisting of the union of the two disks with the centers

$$w_1 = \frac{1}{6}, \quad w_2 = \frac{5}{6},$$

and the radius r , where $0 < r \leq w_1 = 1/6$. Denote by

$$G = \{z : |z - 1/6| > r \text{ and } |z - 5/6| > r\}$$

the complement of D_1 in the extended complex plane. Then $z \mapsto z - \frac{1}{2}$ maps G onto the domain $\widehat{G} = \{z : |z + 1/3| > r \text{ and } |z - 1/3| > r\}$, and it follows from [22, Theorem 5.2.3] and [27, Theorem 4.2] (see also [14, Example 4.6]) that

$$\text{cap}(D_1) = \text{cap}(\widehat{G}^c) = \frac{2K}{\pi} \sqrt{(1/3)^2 - r^2} \sqrt{2L(1 + L^2)} = \frac{2K}{3\pi} \sqrt{1 - 9r^2} \sqrt{2L(1 + L^2)}, \quad (23)$$

where

$$K = K(L^2) = \int_0^1 \frac{1}{\sqrt{(1-t^2)(1-L^4 t^2)}} dt, \quad L = 2\rho \prod_{k=1}^{\infty} \left(\frac{1 + \rho^{8k}}{1 + \rho^{8k-4}} \right)^2,$$

and

$$\rho = \frac{\sqrt{1/3 + r} - \sqrt{1/3 - r}}{\sqrt{1/3 + r} + \sqrt{1/3 - r}} = \frac{\sqrt{1 + 3r} - \sqrt{1 - 3r}}{\sqrt{1 + 3r} + \sqrt{1 - 3r}} = \frac{3r}{1 + \sqrt{1 - 9r^2}}.$$

Thus, for $r \ll 1/6$ we have

$$\rho \approx 3r/2, \quad L \approx 2\rho \approx 3r \ll 1,$$

hence

$$K = K(L^2) \approx K(0) = \frac{\pi}{2},$$

and now (23) implies that

$$\text{cap}(D_1) \approx \frac{1}{3} \times 1 \times \sqrt{2L} \approx \frac{1}{3} \sqrt{6r} = \sqrt{\frac{2r}{3}} \quad (\text{for } r \ll 1/6). \quad (24)$$

For the CSM we set up the linear algebraic system (22) with the system matrix

$$A = - \begin{bmatrix} \log r & \log |w_1 - w_2| \\ \log |w_2 - w_1| & \log r \end{bmatrix} = \begin{bmatrix} -\log r & -\log \frac{2}{3} \\ -\log \frac{2}{3} & -\log r \end{bmatrix}$$

from (17), so that

$$A^{-1} = \frac{1}{(\log r)^2 - (\log \frac{2}{3})^2} \begin{bmatrix} -\log r & \log \frac{2}{3} \\ \log \frac{2}{3} & -\log r \end{bmatrix},$$

and hence (see (21))

$$c = -\frac{(\log r)^2 - (\log \frac{2}{3})^2}{2(\log r - \log \frac{2}{3})} = -\frac{1}{2} \left(\log r + \log \frac{2}{3} \right) = -\frac{1}{2} \log \frac{2r}{3}. \quad (25)$$

Consequently, the CSM estimate is

$$\text{cap}(D_1) \approx \exp(-c) = \exp\left(\frac{1}{2} \log \frac{2r}{3}\right) = \sqrt{\frac{2r}{3}}. \quad (26)$$

Comparing (24) and (26) shows that the CSM gives very accurate results for $r \ll 1/6$. This conclusion is illustrated in Figure 2, where the (blue) solid line shows that the error between the exact capacity (23) and the CSM estimate (26) is 2.87×10^{-18} for $r = 10^{-7}$, but increases to 0.01 for $r = 1/6$.

We next consider the bound (5) from Lemma 2.1, i.e., the inequality

$$|\text{cap}(D_1) - e^{-c}| \leq e^{-c} \left(M + \frac{1}{2} M^2 e^M \right), \quad (27)$$

where $M = |\hat{c} - c| \leq \max_{\zeta \in \partial G} |h(\zeta)| = \max_{\zeta \in \partial D_1} |h(\zeta)|$, and

$$h(z) = c + p_1 \log |z - w_1| + p_2 \log |z - w_2|, \quad z \in G.$$

Here, c is given by (25), $\text{cap}(D_1)$ is given by (23), $\hat{c} = -\log(\text{cap}(D_1))$, and $[p_1, p_2]^T$ is the solution of the linear algebraic system (16), i.e.,

$$\begin{bmatrix} -\log r & -\log \frac{2}{3} \\ -\log \frac{2}{3} & -\log r \end{bmatrix} \begin{bmatrix} p_1 \\ p_2 \end{bmatrix} = \begin{bmatrix} c \\ c \end{bmatrix}.$$

Thus, in view of (25), we have $p_1 = p_2 = 1/2$, and hence

$$h(z) = \frac{1}{2} \log \frac{3}{2r} + \frac{1}{2} \log \left| z - \frac{1}{6} \right| + \frac{1}{2} \log \left| z - \frac{5}{6} \right|,$$

which yields

$$M \leq \max_{\zeta \in \partial D_1} |h(\zeta)| = \frac{1}{2} \log \frac{3}{2} + \frac{1}{2} \log \left(r + \frac{2}{3} \right) = \frac{1}{2} \log \left(\frac{3}{2} r + 1 \right).$$

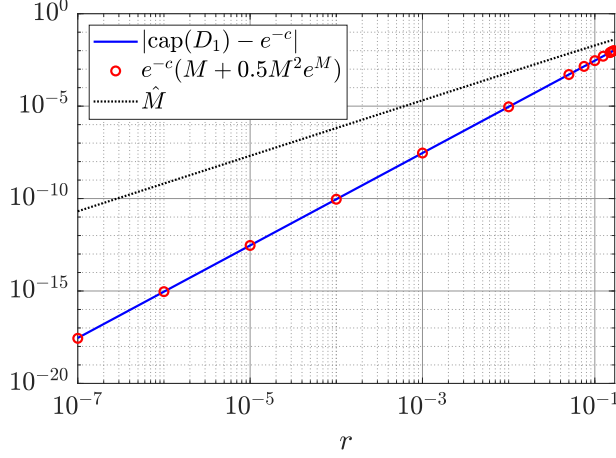


Figure 2: The absolute error $|\text{cap}(D_1) - e^{-c}|$ between the exact capacity $\text{cap}(D_1)$ given by (23) and the CSM estimate e^{-c} in (26), the error bound from Lemma 2.1, and the upper bound \hat{M} in (28).

Using this upper bound on M in (27) we obtain

$$|\text{cap}(D_1) - e^{-c}| \leq \sqrt{\frac{r}{6}} \log\left(\frac{3}{2}r + 1\right) \left(1 + \frac{1}{4} \log\left(\frac{3}{2}r + 1\right) \sqrt{\frac{3}{2}r + 1}\right) =: \hat{M}. \quad (28)$$

The values of the computable upper bound \hat{M} on the absolute error are shown by the dotted line in Figure 2. We observe that for larger values of r the bound becomes quite tight. Figure 2 also shows the error bound $e^{-c}(M + \frac{1}{2}M^2e^M)$, which we can compute in this example since $\text{cap}(D_1)$ is known analytically. Clearly, the bound is very tight in this example.

3.3 Structure and properties of the system matrices

In Section 3.2 we have considered the case of just two disks, and we were able to invert the (2×2) -matrix of the linear algebraic system (22) explicitly. For approximating the logarithmic capacity of the generalized Cantor sets by extrapolating from the values $\text{cap}(D_k)$ for reasonably large k , we will have to solve much larger linear algebraic systems, and thus we need to apply more sophisticated techniques for the numerical solution of (22).

Our first observation in this direction is that the matrix A in (17) is symmetric as well as centrosymmetric, which means that

$$J_m A J_m = A, \quad \text{where} \quad J_m = \begin{bmatrix} & & 1 \\ & \ddots & \\ 1 & & \end{bmatrix} \in \mathbb{R}^{m \times m}.$$

Because of the centrosymmetry, the matrix A can be block-diagonalized with an orthogonal transformation at no additional cost; see [6]. If we partition

$$A = \begin{bmatrix} A_{11} & A_{12} \\ A_{21} & A_{22} \end{bmatrix}, \quad \text{where} \quad A_{11}, A_{22} \in \mathbb{R}^{\frac{m}{2} \times \frac{m}{2}},$$

then

$$A = Q \begin{bmatrix} B & 0 \\ 0 & C \end{bmatrix} Q^T, \quad \text{where} \quad Q = \frac{1}{\sqrt{2}} \begin{bmatrix} I_{m/2} & I_{m/2} \\ J_{m/2} & -J_{m/2} \end{bmatrix} \quad \text{with} \quad Q^T Q = Q Q^T = I_m,$$

and

$$B = A_{11} + A_{12} J_{m/2}, \quad C = A_{11} - A_{12} J_{m/2}. \quad (29)$$

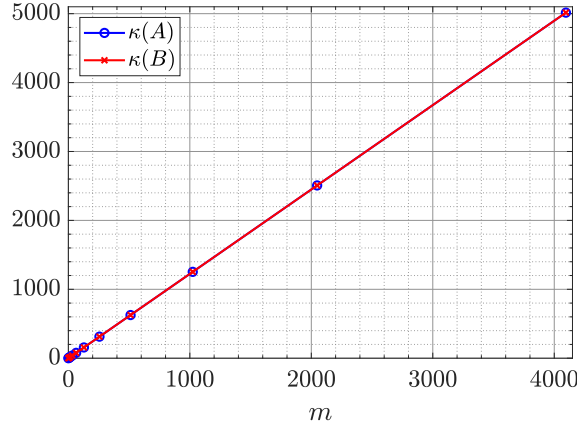


Figure 3: 2-norm condition numbers of $A \in \mathbb{R}^{m,m}$ and $B \in \mathbb{R}^{m/2,m/2}$ from (17) and (29) for $q = 1/3$ as functions of $m = 2^k$, $k = 2, 3, \dots, 12$.

Since A is symmetric, the matrices $B, C \in \mathbb{R}^{\frac{m}{2} \times \frac{m}{2}}$ are also symmetric. If we partition

$$\mathbf{x} = \begin{bmatrix} \mathbf{x}_1 \\ \mathbf{x}_2 \end{bmatrix},$$

and use the orthogonal decomposition of A , then (22) can be transformed via a left-multiplication with Q^T into the equivalent system

$$\begin{bmatrix} B & 0 \\ 0 & C \end{bmatrix} \begin{bmatrix} \mathbf{x}_1 + J_{m/2} \mathbf{x}_2 \\ \mathbf{x}_1 - J_{m/2} \mathbf{x}_2 \end{bmatrix} = \begin{bmatrix} 2\mathbf{e} \\ \mathbf{0} \end{bmatrix},$$

where $\mathbf{e} = [1, \dots, 1]^T \in \mathbb{R}^{m/2}$. Since we assume that A and thus C is nonsingular, the second block row implies that $\mathbf{x}_1 = J_{m/2} \mathbf{x}_2$, and hence it remains to solve the system

$$B\mathbf{y} = \mathbf{e}, \tag{30}$$

where $\mathbf{y} = \mathbf{x}_1$, to obtain $c = 1/(2\mathbf{e}^T \mathbf{y})$. In finite precision, we obtain a computed approximate solution $\tilde{\mathbf{y}} \approx \mathbf{y}$ of (30), which leads to

$$c \approx \frac{1}{2\mathbf{e}^T \tilde{\mathbf{y}}}.$$

Figure 3 shows the 2-norm condition numbers computed in MATLAB¹ of A and B for $q = 1/3$ (i.e., the classical Cantor middle third set) as functions of $m = 2^k$. We observe that the condition numbers grow linearly in m . A similar behavior of the condition numbers can be seen in the Cantor dust example (see Figure 10), and has been observed in [10, Figure 6], where the matrix F in [10, Eq. (36)] has the same form as our matrices A and B . According to [10, p. 398], such behavior of the condition numbers in the CSM is expected, since the matrices “resemble a discretization of the kernel of a single-layer potential whose inverse is the Laplacian operator”. Analyses of the invertibility of matrices in other applications of the CSM can be found in [19].

From a numerical point of view, solving (30) is clearly preferable over solving (22), since B has only half the size of A , while both matrices are dense and have essentially the same condition number (cf. Figure 3). We will solve the linear algebraic system (30) using iterative methods that require one matrix-vector product with B in every step; see Section 3.4. Because of the structure of the entries of B , this multiplication can be

¹All computations in this paper are performed in MATLAB R2017a on an ASUS Laptop with Intel Core i7-8750H CPU @ 2.20GHz, 2208 Mhz, 6 Cores, 12 Logical Processors and 16 GB RAM.

performed using the Fast Multipole Method (FMM) [9]. Using the definition of B in (29), each matrix-vector product of the form $B\mathbf{y} = A_{11}\mathbf{y} + A_{12}J_{m/2}\mathbf{y}$ requires two applications of the FMM. The following result shows that B can be written in a form so that only one application of the FMM is required.

Lemma 3.4. *The entries of B are given by*

$$b_{ij} = \begin{cases} -\log(2r\sqrt{z_i}), & i = j, \\ -\log|z_i - z_j|, & i \neq j, \end{cases} \quad 1 \leq i, j \leq m/2,$$

where $z_i := (w_i - 1/2)^2$ for $i = 1, \dots, m/2$.

Proof. First note that by definition the entries of A_{11} are given by

$$a_{ij} = \begin{cases} -\log r, & i = j, \\ -\log|w_i - w_j|, & i \neq j, \end{cases} \quad 1 \leq i, j \leq m/2,$$

and the entries of A_{12} are given by

$$\hat{a}_{ij} = -\log|w_i - w_{m/2+j}|, \quad 1 \leq i, j \leq m/2.$$

By construction, the w_j , $j = 1, 2, \dots, m$, are real numbers in the interval $(0, 1)$, which are symmetric about $1/2$. Further, we have

$$w_{m/2+j} = 1 - q + w_j, \quad w_{m/2+1-j} + w_j = q, \quad j = 1, \dots, m/2.$$

Thus,

$$\hat{a}_{ij} = -\log|w_i - w_j - 1 + q|, \quad 1 \leq i, j \leq m/2,$$

and hence the entries \tilde{a}_{ij} of the matrix $A_{12}J_{m/2}$ are given by

$$\tilde{a}_{ij} = \hat{a}_{i, m/2+1-j} = -\log|w_i - w_{m/2+1-j} - 1 + q| = -\log|w_i + w_j - 1|, \quad 1 \leq i, j \leq m/2.$$

Finally, by (29), the entries b_{ij} of B are given for $i = j$ by

$$b_{ii} = a_{ii} + \tilde{a}_{ii} = -\log r - \log|2w_i - 1| = -\log|2r(w_i - 1/2)|,$$

and for $i \neq j$ by

$$b_{ij} = a_{ij} + \tilde{a}_{ij} = -\log|w_i - w_j| - \log|w_i + w_j - 1| = -\log|(w_i - 1/2)^2 - (w_j - 1/2)^2|,$$

which completes the proof. \square

From this lemma we have

$$B = - \begin{bmatrix} \log(2r\sqrt{z_1}) & \log|z_1 - z_2| & \cdots & \log|z_1 - z_{m/2-1}| & \log|z_1 - z_{m/2}| \\ \log|z_2 - z_1| & \log(2r\sqrt{z_2}) & \cdots & \log|z_2 - z_{m/2-1}| & \log|z_2 - z_{m/2}| \\ \vdots & \vdots & \ddots & \vdots & \vdots \\ \log|z_{m/2-1} - z_1| & \log|z_{m/2-1} - z_2| & \cdots & \log(2r\sqrt{z_{m/2-1}}) & \log|z_{m/2-1} - z_{m/2}| \\ \log|z_{m/2} - z_1| & \log|z_{m/2} - z_2| & \cdots & \log|z_{m/2} - z_{m/2-1}| & \log(2r\sqrt{z_{m/2}}) \end{bmatrix}, \quad (31)$$

and we can easily see that B is symmetric (as already mentioned above), but not centrosymmetric.

Theorem 3.5. *For $k \geq 2$, the entries b_{ij} of B satisfy*

$$\log \frac{1}{q(1-q)} < \log \frac{1}{(1-q)(q-2r)} \leq b_{ij} \leq \log \frac{1}{r(1-2q+2r)} < \log \frac{1}{r(1-2q)}, \quad (32)$$

and they decay away from the diagonal in each row and column, i.e.,

$$b_{i,1} < \dots < b_{i,i-1} < b_{i,i}, \quad b_{i,i} > b_{i,i+1} > \dots > b_{i,m/2}, \quad (33)$$

$$b_{1,j} < \dots < b_{j-1,j} < b_{j,j}, \quad b_{j,j} > b_{j+1,j} > \dots > b_{m/2,j}, \quad (34)$$

for $1 \leq i, j \leq m/2$.

Proof. In (32), we need $q - 2r > 0$, which is equivalent to $r < q/2$ and thus to $k \geq 2$.

Decay. Since

$$0 < r = w_1 < w_2 < \dots < w_{m/2} = q - r < q < \frac{1}{2}, \quad (35)$$

we have

$$1/4 > z_1 > z_2 > \dots > z_{m/2} > 0. \quad (36)$$

This implies

$$|z_i - z_1| > |z_i - z_2| > \dots > |z_i - z_{i-1}|, \quad |z_i - z_{i+1}| < \dots < |z_i - z_{m/2}|,$$

and equivalently

$$b_{i,1} < \dots < b_{i,i-1}, \quad b_{i,i+1} > \dots > b_{i,m/2}.$$

It remains to show $b_{i,i\pm 1} < b_{ii}$, which is equivalent to $|z_i - z_{i\pm 1}| > 2r\sqrt{z_i}$. Note that

$$|z_i - z_j| = |w_i - w_j||w_i + w_j - 1| = |w_i - w_j|(1 - (w_i + w_j)).$$

Since $|w_i - w_{i-1}| > r$ and $w_i + w_{i-1} < 2w_i < 1$, we have $|z_i - z_{i-1}| > r(1 - 2w_i) = 2r\sqrt{z_i}$, i.e., $b_{i,i-1} < b_{ii}$. Since $|w_i - w_{i+1}| > 2r$, we have

$$|z_i - z_{i+1}| > 2r(1 - (w_i + w_{i+1})) > r(1 - 2w_i).$$

The last estimate is equivalent to $1 > 2w_{i+1}$, which holds by (35). This, together with $2r\sqrt{z_i} = r|2w_i - 1| = r(1 - 2w_i)$, establishes $b_{ii} > b_{i,i+1}$. We thus have shown (33). Since B is symmetric, (33) is equivalent to (34).

Bounds for b_{ij} . Let $1 \leq i, j \leq m/2$. To establish the upper bound, it is enough to show $b_{ii} \leq \log \frac{1}{r(1-2q+2r)}$, which is equivalent to $1 - 2q + 2r \leq 2\sqrt{z_i} = 1 - 2w_i$ and to $w_i \leq q - r$, which holds by (35). Next, we show the lower bound for b_{ij} . It follows from (36) that

$$|z_i - z_j| \leq |z_1 - z_{m/2}|.$$

By (35), we have $z_1 = (0.5 - w_1)^2 = (0.5 - r)^2$ and $z_{m/2} = (0.5 - w_{m/2})^2 = (0.5 - q + r)^2$. Thus

$$|z_i - z_j| \leq |(0.5 - r)^2 - (0.5 - q + r)^2| = |(q - 2r)(1 - q)|$$

and hence, for $i \neq j$,

$$b_{ij} = -\log |z_i - z_j| \geq -\log |(q - 2r)(1 - q)|.$$

The latter inequality holds also for b_{ii} since it is the largest element in its row. The rest is clear. \square

Let $\hat{\mathbf{y}} = B\mathbf{y}$ where $\mathbf{y} = [y_1, \dots, y_{m/2}]^T$ and $\hat{\mathbf{y}} = [\hat{y}_1, \dots, \hat{y}_{m/2}]^T$. In general, computing the vector $\hat{\mathbf{y}}$ requires $O(m^2)$ operations. However, for real \mathbf{y} , the form of B in (31) yields

$$\hat{y}_j = -\log(2r\sqrt{z_j})y_j - \operatorname{Re} \left(\sum_{\substack{\ell=1 \\ \ell \neq j}}^{m/2} y_\ell \log(z_j - z_\ell) \right), \quad j = 1, 2, \dots, m/2, \quad (37)$$

and hence computing the vector $\hat{\mathbf{y}}$ requires one application of the FMM, which uses only $O(m)$ operations; see [9]. In MATLAB, the sum in (37) can be computed fast and efficiently using the MATLAB function `cfmm2dpart` from the toolbox FMMLIB2D [8]. Using the input parameters \mathbf{y} , $\mathbf{z} = [z_1, \dots, z_{m/2}]^T$ and r , the vector $\hat{\mathbf{y}} = B\mathbf{y}$ can be computed by calling the following MATLAB function:

```
function yt = By_eval(y, z, r, iprec)
a(1, :) = real(z); a(2, :) = imag(z);
[U] = cfmm2dpart(iprec, length(z), a, 1, y(:).', 0, [], 1);
yt = -(log(2*r*sqrt(abs(z.')))).*y + real(U.pot).';
end
```

Here, `iprec` is the precision flag for the FMM. In our computations, we use `iprec=4`, which means that the tolerance for the FMM is 0.5×10^{-12} .

3.4 Iteratively solving the linear algebraic systems

As mentioned above, the matrix B is symmetric and nonsingular. Thus, we can apply the MINRES method [21] (which is well defined for symmetric nonsingular matrices) and the GMRES method [26] (which is well defined for all nonsingular matrices) in order to solve the system (30) iteratively². The two methods are mathematically equivalent and minimize the Euclidean residual norm over a sequence of Krylov subspaces in every step. More precisely, when started with the initial vector $\mathbf{y}_0 = 0$, they generate iterates

$$\mathbf{y}_j \in \mathcal{K}_j(B, \mathbf{e}) = \text{span}\{\mathbf{e}, B\mathbf{e}, \dots, B^{j-1}\mathbf{e}\},$$

such that

$$\|\mathbf{e} - B\mathbf{y}_j\|_2 = \min_{\mathbf{z} \in \mathcal{K}_j(B, \mathbf{e})} \|\mathbf{e} - B\mathbf{z}\|_2.$$

Each method is based on generating an orthonormal basis of the Krylov subspaces $\mathcal{K}_j(B, \mathbf{e})$ for $j = 1, 2, \dots$, and this process requires one matrix-vector product with B in every step, which can be computed using the FMM as described above.

The essential difference between the two methods is that MINRES uses the symmetry of the system matrix in order to generate the orthonormal Krylov subspace bases with short (3-term) recurrences, while GMRES is based on full recurrences. Thus, the computational cost of a MINRES step (in terms of memory requirements and floating point operations) is significantly lower than of a GMRES step. However, methods based on short recurrences explicitly perform the orthogonalization only with respect to a few recent vectors. In finite precision computations this can lead to a much faster overall loss of orthogonality, and even a loss of rank in the computed Krylov subspace “basis”. Such loss of rank corresponds to a delay of convergence; see, e.g., [16] or [15, Section 5.9] for comprehensive analyses of this phenomenon and further references.

In the application in this paper the observed delay of convergence is so severe that MINRES is not competitive with GMRES, although it is based on short recurrences.

Example 3.6. We apply the MATLAB implementations of MINRES and GMRES with the initial vector $\mathbf{y}_0 = 0$ to linear algebraic systems of the form (30) for $q = 1/3$ with $m = 2^{14}$ and $m = 2^{16}$. The matrix-vector products with B are performed using the function `By_eval` described above, and hence our function calls to the iterative methods are

```
minres(@(y) By_eval(y, z, r, 4), ones(m/2, 1), tol, MAXIT);
gmres(@(y) By_eval(y, z, r, 4), ones(m/2, 1), [], tol, MAXIT);
```

Our tolerance for the relative residual norm is `tol=1e-12` and we use `MAXIT=400` as the maximal number of iterations, but this number is not reached in our experiment. In Figure 4 we plot the relative residual norms of the two methods. In exact arithmetic these norms are identical. In our finite precision computation we observe that MINRES suffers from a significant delay of convergence. This delay not only leads to many more iterative steps until the tolerance is reached, but also to a much longer computation time in comparison with GMRES:

	GMRES time (s)	MINRES time (s)
$m = 2^{14}$	1.91	3.14
$m = 2^{16}$	8.00	15.46

As a consequence of these numerical observations we have decided to use GMRES in all our experiments.

²Numerical experiments suggest that the matrix A and hence also B are positive definite. We did not prove this, but we performed numerical experiments also with the CG method [11] applied to the system (30), and in these experiments the CG residual norms behaved similarly to those of MINRES.

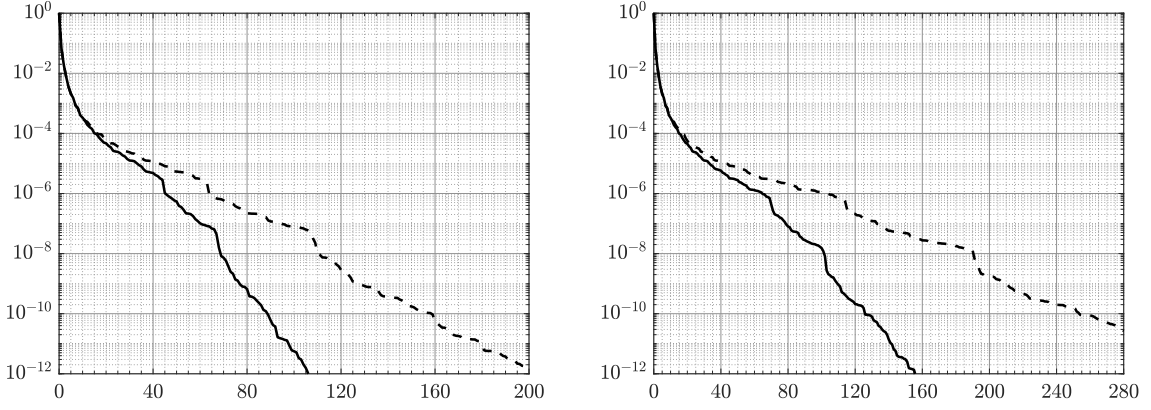


Figure 4: Relative residual norms of GMRES (solid) and MINRES (dashed) for the linear algebraic systems (30) for $q = 1/3$ with $m = 2^{14}$ (left) and $m = 2^{16}$ (right) in Example 3.6.

We will now describe a problem-adapted technique to precondition the system (30), which will lead to an even faster convergence of GMRES. Consider the matrix A in (17) for a fixed size $m = 2^k$. Because of the symmetric distribution of the w_j , $j = 1, \dots, m$, for any fixed $j = 1, \dots, k-1$ we can write this matrix in the block form

$$A = - \begin{bmatrix} D & D_{12} & \cdots & D_{1p} \\ D_{21} & D & \ddots & \vdots \\ \vdots & \ddots & \ddots & D_{p-1,p} \\ D_{p1} & \cdots & D_{p,p-1} & D \end{bmatrix}, \quad \text{where } D \in \mathbb{R}^{2^j \times 2^j}, \text{ and } p = 2^{k-j}. \quad (38)$$

By construction, the entries of A decay row- and column-wise with their distance from the diagonal; see Theorem 3.3. Hence the “block diagonal part” $P_m := \text{diag}(D, \dots, D)$ contains the largest entries of A . This block diagonal matrix is easy to invert when j is not too large, since it requires just one inversion of D . Hence it can be used as a preconditioner for the linear algebraic system (22).

From (29) we have $B = A_{11} + A_{12}J_{m/2}$, where A_{11} is the leading $(\frac{m}{2} \times \frac{m}{2})$ -block of A , and A_{12} is the upper off-diagonal block, which overall contains smaller entries than A_{11} . The “block diagonal part” of A_{11} contains $p/2$ copies of D . We use this matrix

$$P_{m/2} := \text{diag}(D, \dots, D) \in \mathbb{R}^{\frac{m}{2} \times \frac{m}{2}}$$

as our preconditioner for the system (30) with B , i.e., instead of (30) we apply GMRES to the system

$$P_{m/2}^{-1}B\mathbf{y} = P_{m/2}^{-1}\mathbf{e}. \quad (39)$$

The effectiveness of this approach is illustrated next.

Example 3.7. We consider the same linear algebraic systems as in Example 3.6. Figure 5 shows the relative residual norms of GMRES applied to the system $B\mathbf{y} = \mathbf{e}$ (solid) and the preconditioned system $P_{m/2}^{-1}B\mathbf{y} = P_{m/2}^{-1}\mathbf{e}$ (dotted), where we have used $j = 4$ for the preconditioner $P_{m/2}$, and have inverted the matrix $D \in \mathbb{R}^{16 \times 16}$ explicitly using MATLAB’s `inv` function. The solid curves in Figure 5 are the same as in Figure 4. We observe that the preconditioning reduces the number of GMRES iterations to reach the relative residual norm tolerance of 10^{-12} by more than 50%, and that the required times are reduced accordingly:

	GMRES time (s)	Preconditioned GMRES time (s)
$m = 2^{14}$	1.91	0.98
$m = 2^{16}$	8.00	3.83

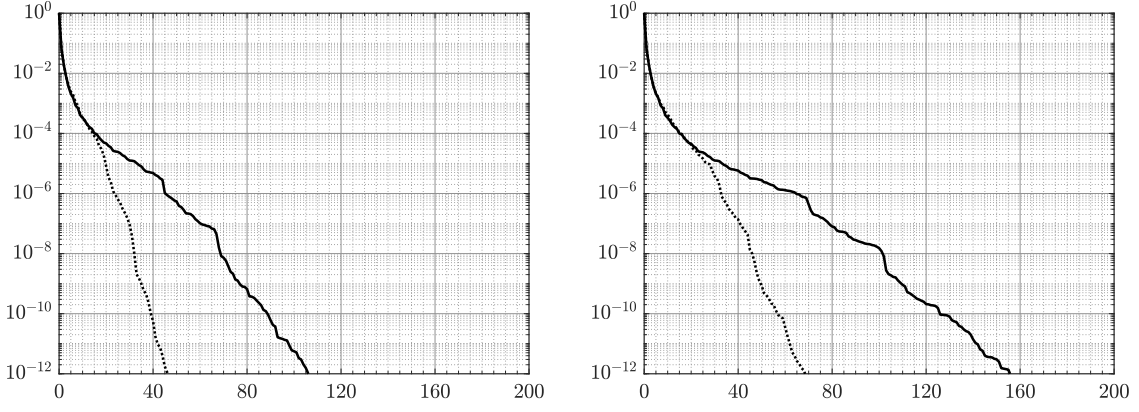


Figure 5: Relative residual norms of GMRES (solid) and preconditioned GMRES (dotted) with $m = 2^{14}$ (left) and $m = 2^{16}$ (right) in Example 3.7.

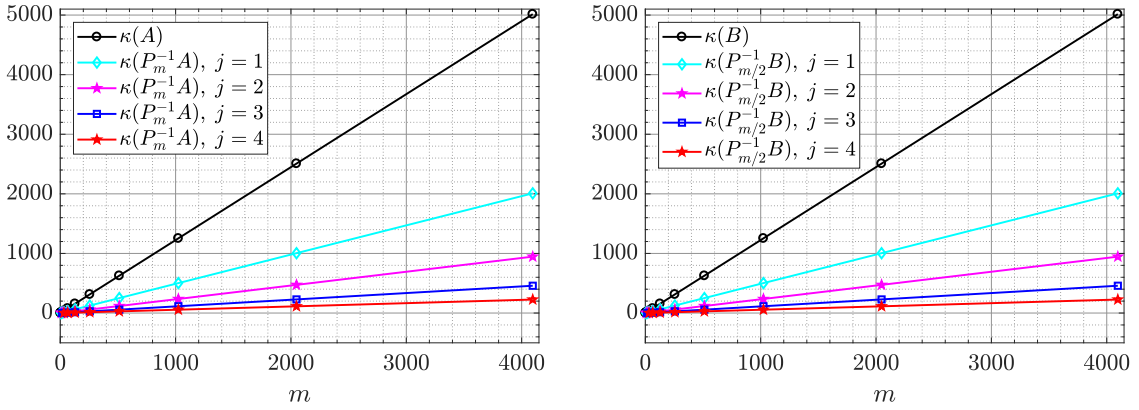


Figure 6: 2-norm condition numbers of the matrices $P_m^{-1}A \in \mathbb{R}^{m,m}$ and $P_{m/2}^{-1}B \in \mathbb{R}^{m/2,m/2}$ as functions of $m = 2^k$ for $q = 1/3$, $j = 1, 2, 3, 4$, and $k = j + 1, j + 2, \dots, 12$.

The effect of the preconditioner on the matrix condition number can be seen in Figure 6, where we show the condition numbers of $P_m^{-1}A$ and $P_{m/2}^{-1}B$ as functions of m for several values of j . The results presented in Figure 7 suggest that

$$\frac{\kappa(P_m^{-1}A)}{\kappa(A)} \approx \frac{1}{2^{j+1/2}} \quad \text{and} \quad \frac{\kappa(P_{m/2}^{-1}B)}{\kappa(B)} \approx \frac{1}{2^{j+1/2}}.$$

Clearly, the condition numbers of the preconditioned matrices decrease with increasing j , while a larger j leads to higher computational costs for applying the preconditioner. In our experiments we found that $j = 4$ represents a good trade-off value. For this value we have $\frac{\kappa(P_m^{-1}A)}{\kappa(A)} \approx 0.045$ and $\frac{\kappa(P_{m/2}^{-1}B)}{\kappa(B)} \approx 0.045$.

Using the preconditioner $P_{m/2}$, the above MATLAB function `By_eval` is modified as follows:

```
function yt = By_peval(y, z, r, iprec, invD)
a(1, :) = real(z); a(2, :) = imag(z);
[U] = cfmm2dpart(iprec,length(z),a,1,y(:).',0,[],1);
yt = -(log(2*r*sqrt(abs(z.')))).*y + real(U.pot).';
[dD, dD] = size(invD);
for k=1:length(z)/dD
    yt(dD*(k-1)+1:dD*k) = invD*yt(dD*(k-1)+1:dD*k);
end
end
```

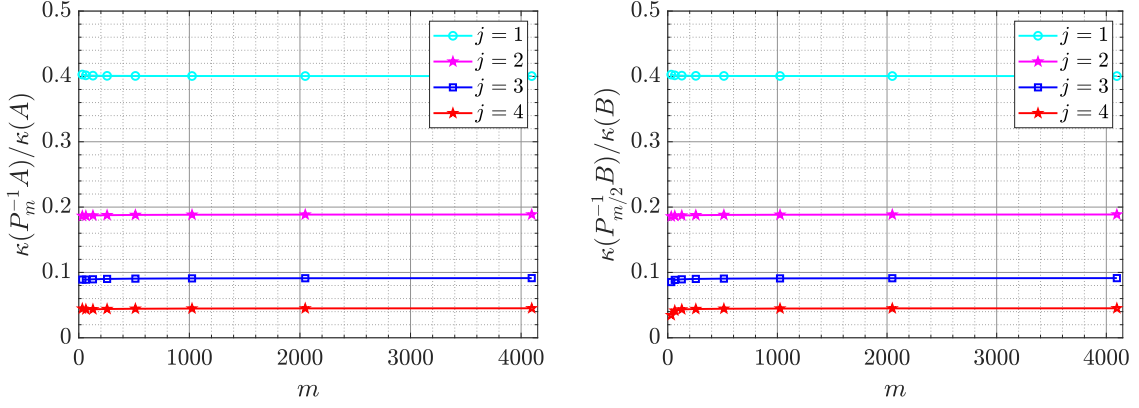


Figure 7: $\kappa(P_m^{-1}A)/\kappa(A)$ and $\kappa(P_{m/2}^{-1}B)/\kappa(B)$ as functions of $m = 2^k$ for $q = 1/3$, $j = 1, 2, 3, 4$, and $k = 5, 6, \dots, 12$.

3.5 Computing the logarithmic capacity of generalized Cantor sets

We now present the results of numerical computations with the method described above for computing the logarithmic capacity of generalized Cantor sets. Our method requires the parameters q (for the definition of the generalized Cantor set) and k (for the level of the approximation) as its only inputs; see (6). These parameters completely determine the preconditioned linear algebraic system (39) that we solve with GMRES, where the matrix-vector products are computed using the FMM as described above. As in the examples above, the tolerance for the relative GMRES residual norm is 10^{-12} . GMRES then returns a computed approximation $\tilde{\mathbf{y}} \approx \mathbf{y}$, and we report the value $\exp(-1/(2e^T \tilde{\mathbf{y}}))$ as $\text{cap}(D_k)$ in our tables below.

Example 3.8 (Classical Cantor middle third set). We consider the classical Cantor middle third set, i.e., the set (7) with $q = 1/3$ in (6). Table 1 gives the approximate values of $\text{cap}(D_k)$ for $k = 5, 6, \dots, 20$ computed by the method presented in this paper, as well as the computation time (in seconds), and the number of GMRES iteration steps.

We compare these results with the computed values and the corresponding timings for the BIE method from [14]. Approximating $\text{cap}(E_k)$ with the BIE method requires a preliminary conformal map to “open up” the intervals of E_k to obtain a compact set of the same capacity, but bounded by smooth Jordan curves. Then the method is used to compute the capacity of this new set. For approximating $\text{cap}(D_k)$ with the BIE method, no preliminary conformal map is needed since ∂D_k is smooth. For both cases, we take $n = 2^6$ discretization points on each of the $m = 2^k$ boundary curves, and the obtained results are presented in Table 2. (The value $n = 2^6$ was chosen, since with this value the BIE method yields the logarithmic capacity of a single disk and of two disks with equal radius with a relative error of order 10^{-16} .) Further, by Tables 1 and 2, there is a good agreement between the approximations of $\text{cap}(D_k)$ obtained by the BIE method from [14] and the method presented in this paper. This agreement improves as k increases. As described in Remark 3.2, the new method is significantly more efficient, since it uses only a single charge point for each component of D_k . In addition, we have used the special (centrosymmetric) structure of the system matrices as well as a preconditioner for GMRES to speed up the computations.

The estimate of $\text{cap}(E)$ in [14] was obtained by extrapolation from the computed values for $\text{cap}(E_k)$. Using the same approach here, we start by noting that the differences

$$d_k = \text{cap}(D_k) - \text{cap}(D_{k+1}), \quad k = 5, 6, \dots, 19,$$

decrease linearly on a logarithmic scale. We store these 15 values in the vector d , and use the MATLAB command `p=polyfit(5:19,log(d),1)` to compute a linear polynomial

Table 1: Computed approximations of $\text{cap}(D_k)$ for $q = 1/3$, timings, and number of GMRES iteration steps using the new proposed method for Example 3.8.

k	$m = 2^k$	$\text{cap}(D_k)$	time (s)	iter
5	32	0.227457816902705	0.03	4
6	64	0.224254487425132	0.03	7
7	128	0.222633059381908	0.06	10
8	256	0.221808427761487	0.11	15
9	512	0.221387991441743	0.16	19
10	1024	0.221173357505459	0.22	22
11	2048	0.221063713734092	0.27	25
12	4096	0.221007684178946	0.40	32
13	8192	0.220979047273590	0.68	39
14	16384	0.220964409542387	1.00	47
15	32768	0.220956927135913	1.70	57
16	65536	0.220953102245645	3.37	69
17	131072	0.220951146997627	7.95	81
18	262144	0.220950147487058	16.79	97
19	524288	0.220949636541913	37.79	119
20	1048576	0.220949375348718	96.98	143

Table 2: Computed approximations of $\text{cap}(E_k)$ and $\text{cap}(D_k)$ for $q = 1/3$, and timings using the BIE Method [14] for Example 3.8.

k	$m = 2^k$	$\text{cap}(E_k)$	time (s)	$\text{cap}(D_k)$	time (s)
5	32	0.221938129124324	9.95	0.227918836283900	4.69
6	64	0.221454205006181	19.24	0.224486551122397	12.67
7	128	0.221207178734289	47.21	0.222750783871879	40.66
8	256	0.221080995391656	131.18	0.221868377621828	111.86
9	512	0.221016516406109	402.66	0.221418578408387	357.10
10	1024	0.220983561713855	1405.82	0.221188978166610	1277.74
11	2048	0.220966717159289	5071.78	0.221071694998756	4351.78
12	4096	0.220958106742622	18207.76	0.221011763144866	15509.24

$p(x) = p_1x + p_2$ of best approximation in the least squares sense for the values $\log(d_k)$. The computed coefficients are

$$p_1 = -0.671894676421546, \quad p_2 = -2.39546038319728.$$

Starting with our computed approximation of $\text{cap}(D_{20})$ we can then approximate $\text{cap}(D_k)$ for $k \geq 21$ by extrapolation, i.e.,

$$\text{cap}(D_k) \approx \text{cap}(D_{20}) - \sum_{j=20}^{k-1} \exp(p(j)), \quad k \geq 21.$$

Since $\exp(p(52)) < 10^{-16}$, we use this formula with $k = 52$ for our final estimate of $\text{cap}(E)$ which is shown in Table 3. Applying the same extrapolation approach to the values obtained by the BIE method (see Table 2) yields the estimates of $\text{cap}(E)$ presented in Table 3.

Our estimate (obtained with the new proposed method) agrees in its first eight significant digits with the one that was “strongly suggested” by Ransford [23, p. 568]. All

Table 3: Estimates of the logarithmic capacity of the classical Cantor middle third set. Matching digits are underlined.

New Method	<u>0.220949</u> 103628452
BIE Method (based on $\text{cap}(E_k)$)	<u>0.220949</u> 114469744
BIE Method (based on $\text{cap}(D_k)$)	<u>0.220949</u> 728829335
Ransford [23]	<u>0.220949</u> 102189525665
Krüger and Simon [13]	<u>0.220949</u> 98647421

Table 4: The computed approximations of $\text{cap}(E)$ for the generalized Cantor set; see Example 3.9.

q	BIE Method [14]	New Method
4/24	<u>0.1384</u> 4418298159	<u>0.1384</u> 37531550946
6/24	<u>0.1865</u> 11016338442	<u>0.1865</u> 08655120292
8/24	<u>0.220949</u> 194629475	<u>0.220949</u> 103628452
9/24	<u>0.2332</u> 18551525021	<u>0.2332</u> 18660959678
10/24	<u>0.2422</u> 33234580321	<u>0.2422</u> 33644605597
11/24	<u>0.2479</u> 29630663845	<u>0.2479</u> 30030139435

these estimates agree in their first six significant digits, and they are all contained in the interval

$$[0.22094810685, 0.22095089228],$$

which according to Ransford and Rostand [24] contains $\text{cap}(E)$.

Example 3.9 (Generalized Cantor set). We consider now the numerical approximation of $\text{cap}(E)$ for general $q \in (0, 0.5)$. The limiting cases are $E = \{0, 1\}$ with $\text{cap}(E) = 0$ (for $q = 0$) and $E = [0, 1]$ with $\text{cap}(E) = 0.25$ (for $q = 0.5$). For several values of q , we approximate the values of $\text{cap}(D_k)$ with the CSM and extrapolate these values to obtain an approximation of $\text{cap}(E)$ using the same approach as described in Example 3.8. The results are given in Table 4, where the values of q are chosen from the values considered in [14, Example 4.14] (note that q here is denoted by r in [14]). We also state the values of $\text{cap}(E)$ computed in [14] using a discretization with $k = 12$ (corresponding to $m = 4096$), and then extrapolation. We observe that the estimates obtained by the two methods agree at least in their first four significant digits (matching digits are underlined).

It was suggested in [24] that the values of $\text{cap}(E)$ can be approximated by

$$\text{cap}(E) \approx f(q) = q(1 - q) - \frac{q^3}{2} \left(\frac{1}{2} - q \right)^{3/2}. \quad (40)$$

Figure 8 shows the graph of the function $f(q)$ as well as our computed approximations of $\text{cap}(E)$. The maximum distance between the values of $f(q)$ and the computed approximations of $\text{cap}(E)$ from the third column of Table 4 is 7.56×10^{-5} , which is close to the results reported in [14].

4 Cantor dust

The Cantor dust is a generalization of the Cantor set to dimension two. We compute the logarithmic capacity of the generalized Cantor dust, and start by setting up the CSM, similarly to our approach in Section 3.

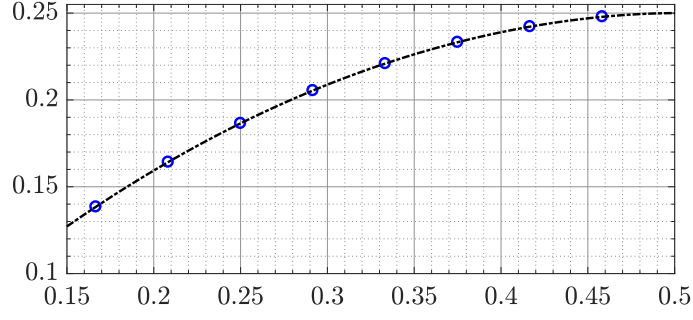


Figure 8: The computed logarithmic capacity $\text{cap}(E)$ (blue circles) and $f(q)$ from (40) (dashed); see Example 3.9.

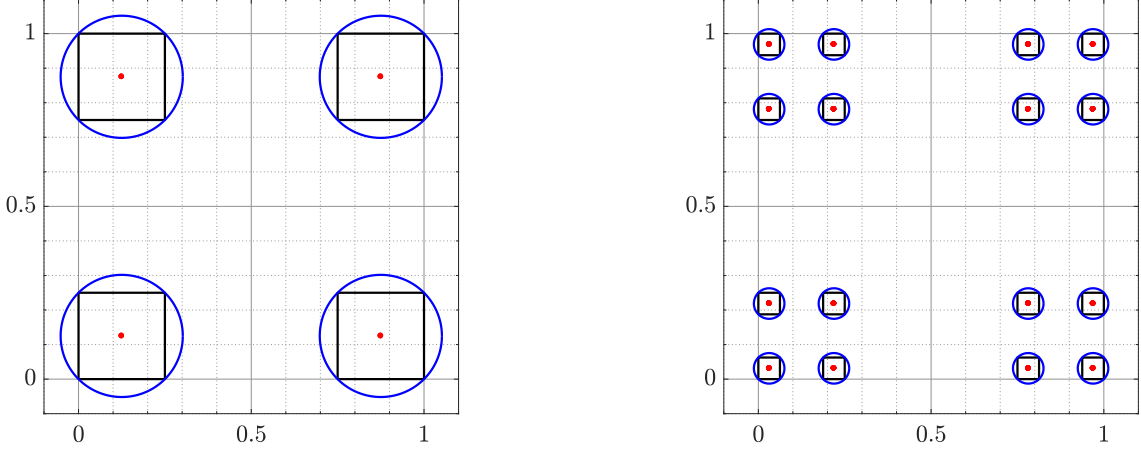


Figure 9: The Cantor dust with $q = 1/4$ for $k = 1$ (left) and $k = 2$ (right).

Let $q \in (0, 1/2)$ and $F_0 = [0, 1] \times [0, 1]$. Define recursively

$$F_k := qF_{k-1} \cup (qF_{k-1} + 1 - q) \cup (qF_{k-1} + (1 - q)i) \cup (qF_{k-1} + (1 - q)(1 + i)), \quad k \geq 1,$$

i.e., $F_k = E_k \times E_k$ with E_k from (6). Then the generalized Cantor dust F is defined as

$$F := \bigcap_{k=0}^{\infty} F_k. \quad (41)$$

Note that F_k consists of $m = 4^k$ closed square regions, say $S_{k,1}, S_{k,2}, \dots, S_{k,m}$; see Figure 9 for $q = 1/4$ with $k = 1$ (left) and $k = 2$ (right). The diameter of each of the squares $S_{k,1}, S_{k,2}, \dots, S_{k,m}$ is $2r_k$, where

$$r_k := \frac{1}{\sqrt{2}} q^k. \quad (42)$$

For $j = 1, 2, \dots, m$, denote the center of $S_{k,j}$ by $w_{k,j}$. To be precise, we order the points $w_{k,j}$ recursively by $w_0 = (1 + i)/2$ and

$$w_k = [w_{k,j}] = [qw_{k-1}, qw_{k-1} + (1 - q), qw_{k-1} + (1 - q)i, qw_{k-1} + (1 - q)(1 + i)] \in \mathbb{C}^{1,4^k} \quad (43)$$

for $k \geq 1$. Let $D_{k,j}$ be the disk with center $w_{k,j}$ and radius r_k , and let

$$D_k = \bigcup_{j=1}^m D_{k,j};$$

see Figure 9 for $q = 1/4$ with $k = 1$ (left) and $k = 2$ (right).

Theorem 4.1. *Let F be the Cantor dust defined by (41), then*

$$\bigcap_{k=0}^{\infty} D_k = F \quad \text{and} \quad \text{cap}(F) = \lim_{k \rightarrow \infty} \text{cap}(D_k).$$

Proof. By construction, $F_k \subseteq D_k$ for all $k \in \mathbb{N}_0$, hence $F \subseteq \bigcap_{k=0}^{\infty} D_k$. If $z \in \mathbb{C} \setminus F$, then there exists $k_0 \in \mathbb{N}$ with $z \notin F_{k_0}$. In particular, $d := \text{dist}(z, F_{k_0}) > 0$ since F_{k_0} is compact. Since the maximal distance from a point on $\partial D_{k,j}$ to the inscribed square $S_{k,j}$ is $r_k - \frac{1}{2}q^k = \frac{\sqrt{2}-1}{2}q^k \rightarrow 0$ for $k \rightarrow \infty$, we have $z \notin D_{k_1}$ for a sufficiently large k_1 , hence $z \notin \bigcap_{k=0}^{\infty} D_k$. Finally, $\text{cap}(F) = \lim_{k \rightarrow \infty} \text{cap}(D_k)$ by [22, Theorem 5.1.3], since $D_0 \supseteq D_1 \supseteq D_2 \supseteq \dots$ are compact and $F = \bigcap_{k=0}^{\infty} D_k$. \square

As in Section 3, we first approximate $\text{cap}(D_k)$ for several k with the CSM, and then extrapolate these values to obtain an approximation of $\text{cap}(F)$. With the choice (42) of r_k , and to make sure the disks $D_{k,j}$, $j = 1, 2, \dots, 4^k$, are disjoint, we will consider here only the case $q < \sqrt{2} - 1$. Then the complement of D_k , denoted by $G_k = (\mathbb{C} \cup \{\infty\}) \setminus D_k$, is an unbounded multiply connected domain of connectivity $m = 4^k$ with

$$\partial G_k = \partial D_{k,1} \cup \dots \cup \partial D_{k,4^k}.$$

We parametrize the circle $\partial D_{k,j}$ by $\eta_{k,j}(t) = w_{k,j} + r_k e^{it}$, $0 \leq t \leq 2\pi$, for $j = 1, 2, \dots, 4^k$.

As described in Section 3, we approximate the Green's function of G_k by a function h_k of the form (11) with (12). The condition (13) leads to the linear algebraic system (16) with the matrix $A \in \mathbb{R}^{m,m}$ from (17), now with $m = 4^k$ instead of 2^k , which is symmetric and centrosymmetric. Then

$$\text{cap}(D_k) \approx e^{-c_k} \quad \text{where} \quad c_k = \frac{1}{\mathbf{e}^T A^{-1} \mathbf{e}}.$$

As before, we solve $A\mathbf{x} = \mathbf{e}$ to obtain c_k as $c_k = 1/(\mathbf{e}^T \mathbf{x})$. Note that the estimates of the entries of A in Theorem 3.3 do not carry over from the case of the generalized Cantor set to the generalized Cantor dust.

We will now fix $m = 4^k$ and drop the index k in the following for simplicity. The matrix A for the generalized Cantor dust has the same structure as the matrix A for the generalized Cantor set. In particular, using that A is centrosymmetric, we can reduce the linear system $A\mathbf{x} = \mathbf{e}$ of size m to the system

$$B\mathbf{y} = \mathbf{e}$$

of size $m/2$, where B is given by (29), and obtain

$$c = \frac{1}{2\mathbf{e}^T \mathbf{y}} \approx \frac{1}{2\mathbf{e}^T \tilde{\mathbf{y}}},$$

where $\tilde{\mathbf{y}}$ is a computed approximate solution to $B\mathbf{y} = \mathbf{e}$, as described in Section 3.3. The following analog of Lemma 3.4 for the generalized Cantor dust allows to compute a multiplication with B with a single application of the FMM.

Lemma 4.2. *The entries of $B = [b_{ij}] \in \mathbb{R}^{m/2, m/2}$ are given by*

$$b_{ij} = \begin{cases} -\log|2r_k\sqrt{z_i}|, & i = j, \\ -\log|z_i - z_j|, & i \neq j, \end{cases} \quad 1 \leq i, j \leq m/2,$$

where $z_i := (w_i - (1+i)/2)^2$ for $i = 1, \dots, m/2$, and r_k is given by (42).

Proof. The entries of the matrix A_{11} are given by

$$a_{ij} = \begin{cases} -\log r_k, & i = j, \\ -\log |w_i - w_j|, & i \neq j, \end{cases}$$

for $1 \leq i, j \leq m/2$. The entries of the matrix A_{12} are given by

$$\hat{a}_{ij} = -\log |w_i - w_{m/2+j}|, \quad 1 \leq i, j \leq m/2.$$

Unlike the generalized Cantor set, here the points w_j , $j = 1, 2, \dots, m$, are complex numbers in the square domain $(0, 1) \times (0, 1)$. By the definition (43) of the points w_j , we have

$$w_{m/2+j} = (1-q)i + w_j, \quad w_{m/2+1-j} + w_j = 1 + qi, \quad \text{for } 1 \leq j \leq m/2.$$

Thus,

$$\hat{a}_{ij} = -\log |w_i - w_j - (1-q)i|, \quad 1 \leq i, j \leq m/2,$$

and hence the entries \tilde{a}_{ij} of the matrix $A_{12}J_{m/2}$ are given by

$$\tilde{a}_{ij} = \hat{a}_{i, m/2+1-j} = -\log |w_i - w_{m/2+1-j} - (1-q)i| = -\log |w_i + w_j - 1 - i|, \quad 1 \leq i, j \leq m/2.$$

Finally, the entries b_{ij} , $1 \leq i, j \leq m/2$, of the matrix B are given for $i = j$ by

$$b_{ii} = a_{ii} + \tilde{a}_{ii} = -\log r_k - \log |2w_i - 1 - i| = -\log |2r_k(w_i - (1+i)/2)| = -\log |2r_k \sqrt{z_i}|,$$

and for $i \neq j$ by

$$b_{ij} = a_{ij} + \tilde{a}_{ij} = -\log |w_i - w_j| - \log |w_i + w_j - 1 - i| = -\log |z_i - z_j|,$$

as claimed. \square

The matrix B is symmetric but not centrosymmetric. Similarly to the approach for the generalized Cantor set in Section 3.4, the condition number of B grows linearly with m ; see Figure 10. We solve $By = \mathbf{e}$ with GMRES and construct a left preconditioner for the matrices A and B in the case of the generalized Cantor dust. For $j = 1, 2, \dots, k-1$, the matrix A can be written in the block form (38) where now $D \in \mathbb{R}^{4^j \times 4^j}$ and $p = 4^{k-j}$. Define the block-diagonal matrices

$$P_m = \text{diag}(D, \dots, D) \in \mathbb{R}^{m, m} \quad \text{and} \quad P_{m/2} = \text{diag}(D, \dots, D) \in \mathbb{R}^{m/2, m/2},$$

where P_m contains $p = 4^{k-j}$ copies of the matrix D , and $P_{m/2}$ contains $p/2$ copies of D . Then the matrix P_m is used as a preconditioner for the system (22), and the matrix $P_{m/2}$ is used as a preconditioner for the system (30). The condition numbers of the matrices $P_m^{-1}A$ and $P_{m/2}^{-1}B$ is shown in Figure 11 for $j = 1, 2$. In our numerical computation, we consider $j = 2$ and hence the size of the matrix D is 16×16 . In this case, we have $\kappa(P_m^{-1}A) \approx 0.077 \kappa(A)$ and $\kappa(P_{m/2}^{-1}B) \approx 0.077 \kappa(B)$; see Figure 12.

In [17, Corollary 3] it is shown that

$$(1-2q)\sqrt[3]{q} \leq \text{cap}(F) \leq \sqrt{2}\sqrt[3]{q}. \quad (44)$$

For $q = 1/3$ the values of the lower and upper bounds rounded to four significant digits are 0.2311 and 0.9806, respectively. A comparison with (45) below illustrates that we do not expect the bounds (44) to be very tight. We therefore do not further consider them in our numerical examples.

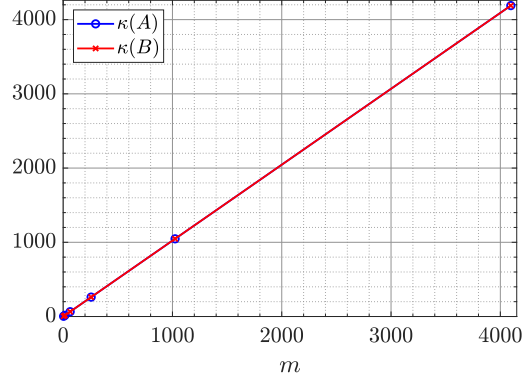


Figure 10: 2-norm condition numbers of $A \in \mathbb{R}^{m,m}$ and $B \in \mathbb{R}^{m/2,m/2}$ from (17) and (29) for the Cantor dust with $q = 1/3$ as functions of $m = 4^k$ for $k = 1, 2, \dots, 7$.

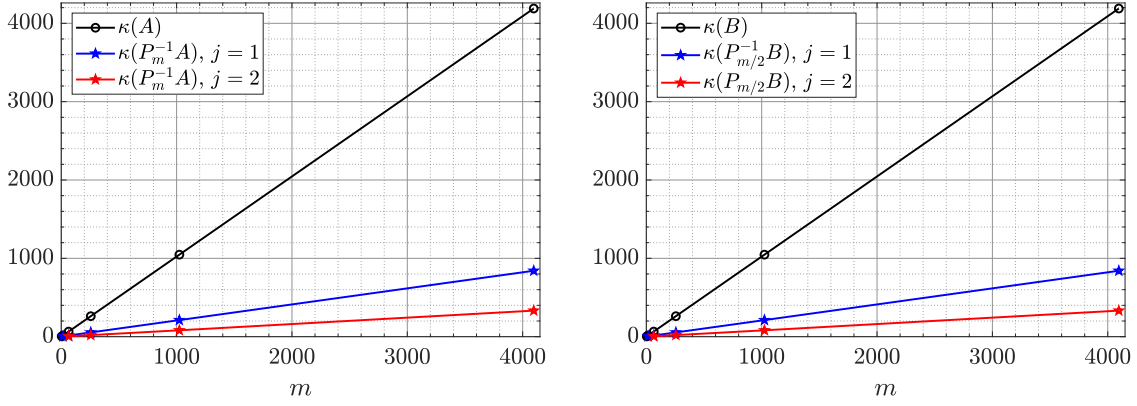


Figure 11: 2-norm condition numbers of $P_m^{-1}A \in \mathbb{R}^{m,m}$ and $P_{m/2}^{-1}B \in \mathbb{R}^{m/2,m/2}$ as functions of $m = 4^k$ for $q = 1/3$, $j = 1, 2$, and $k = j + 1, j + 2, \dots, 6$.

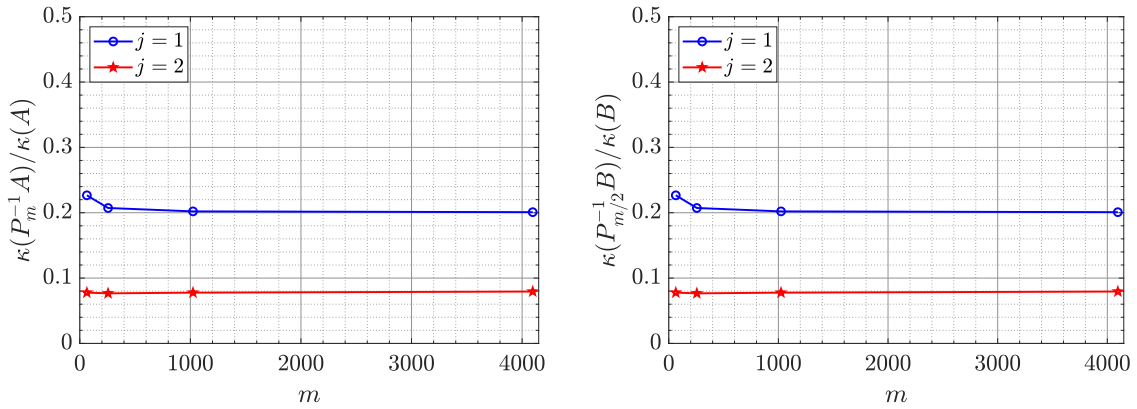


Figure 12: $\kappa(P_m^{-1}A)/\kappa(A)$ and $\kappa(P_{m/2}^{-1}B)/\kappa(B)$ as functions of $m = 4^k$ for $q = 1/3$, $j = 1, 2$, and $k = 3, 4, 5, 6$.

Table 5: The computed approximate values of $\text{cap}(D_k)$ for $q = 1/3$; see Example 4.3.

k	$m = 4^k$	BIE Method [14]		New Method		
		$\text{cap}(D_k)$	time (s)	$\text{cap}(D_k)$	time (s)	iter
1	4	0.624190165168316	0.31	0.560597610169143	0.02	1
2	16	0.592984584624405	2.27	0.569592176189256	0.02	3
3	64	0.581332069392025	13.60	0.572519249447232	0.03	6
4	256	0.576967822959311	164.36	0.573655973612409	0.07	12
5	1024	0.575330169313215	1916.67	0.574085928829936	0.18	25
6	4096	0.574715154920085	31052.23	0.574247683774223	0.42	36
7	16384			0.574308476438467	1.47	54
8	65536			0.574331319690862	6.24	80
9	262144			0.574339902832891	32.13	117
10	1048576			0.574343127837383	202.43	184

Example 4.3 (Classical Cantor middle third dust). The classical Cantor middle third dust is obtained for $q = 1/3$. This example has been considered by Ransford and Rostand in [23, §5.4] where it was proved that

$$\text{cap}(F) \in [0.573550, 0.575095], \quad (45)$$

and their “best guess” is

$$\text{cap}(F) \approx \underline{0.5743450704}. \quad (46)$$

As for the generalized Cantor sets, we compare our new method with the BIE method from [14]. In that method we first approximate $\text{cap}(D_k)$ using $n = 2^6$ discretization points on each boundary component. This leads to linear algebraic systems of size $nm \times nm$, where $m = 4^k$; see Remark 3.2. The computed results and the timings for $k = 1, 2, \dots, 6$ are given in Table 5. Similarly to Example 3.8 we extrapolate the values in Table 5 in order to obtain an approximation of $\text{cap}(F)$. For the approximate values of $\text{cap}(D_k)$ obtained by the BIE method, the differences

$$d_k = \text{cap}(D_k) - \text{cap}(D_{k+1}), \quad k = 1, \dots, 5,$$

decrease linearly on a logarithmic scale. We store these 5 values in the vector d , and use the MATLAB command `p=polyfit(1:5,log(d),1)` to compute a linear polynomial $p(x) = p_1x + p_2$ of best approximation in the least squares sense for the values $\log(d_k)$. The computed coefficients are

$$p_1 = -0.981567064346955, \quad p_2 = -4.487710197832711.$$

Starting with our computed approximation of $\text{cap}(D_6)$ we can then approximate $\text{cap}(D_k)$ for $k \geq 6$ by extrapolation, i.e.,

$$\text{cap}(D_k) \approx \text{cap}(D_6) - \sum_{j=6}^{k-1} \exp(p(j)), \quad k \geq 6.$$

We have $\exp(p(35)) < 10^{-16}$, and hence we use this formula with $k = 35$ for our estimate

$$\text{cap}(F) \approx \underline{0.574347200461138}. \quad (47)$$

Next, we use the new method based on the CSM to compute approximations of $\text{cap}(D_k)$. Since the size of the preconditioner matrix is 16×16 , the method is used without

preconditioning technique for $k < 3$. The method with preconditioning technique is used for $k \geq 3$, so that the size of the linear system is $m \times m$ with $m \geq 64$. Table 5 gives the computed approximations of $\text{cap}(D_k)$, the timings, and the number of GMRES iteration steps for $k = 1, 2, \dots, 10$. We observe that the computed approximations of $\text{cap}(D_k)$ are increasing, although $\text{cap}(D_{k+1}) \leq \text{cap}(D_k)$ (since $D_{k+1} \subset D_k$ for $k \geq 1$). This is most likely due to the fact that we use the CSM with only one point in the interior of each disk $D_{k,j}$, $j = 1, 2, \dots, 4^k$, so that the numerical approximations are not accurate enough to yield a decreasing sequence. As shown in Table 5, the BIE method indeed gives a decreasing sequence of approximations. But here we use $n = 2^6$ discretization points for each circle $\partial D_{k,j}$ for $j = 1, 2, \dots, 4^k$, which results in significantly longer computation times.

For the approximate values of $\text{cap}(D_k)$ obtained with the CSM in Table 5, the differences

$$d_k = \text{cap}(D_{k+1}) - \text{cap}(D_k), \quad k = 1, 2, \dots, 9,$$

decrease linearly on a logarithmic scale. We store these 9 values in the vector d and use the MATLAB command `p=polyfit(1:9,log(d),1)` to compute a linear polynomial

$$p(x) = -0.983339218806568x - 3.806740804822764$$

of best approximation in the least squares sense for the values $\log(d_k)$. Starting with our computed approximation of $\text{cap}(D_{10})$ we approximate $\text{cap}(D_k)$ for $k \geq 11$ by extrapolation, i.e.,

$$\text{cap}(D_k) \approx \text{cap}(D_{10}) + \sum_{j=10}^{k-1} \exp(p(j)), \quad k \geq 11.$$

We have $\exp(p(34)) < 10^{-16}$, and hence we use this formula with $k = 34$ for our estimate

$$\text{cap}(F) \approx \underline{0.574345031687538}. \quad (48)$$

This estimate agrees in its first eight significant digits with the estimate in (46) obtained in [23], and all three estimates stated above agree in their first five significant digits.

Finally, for $q = 1/3$, it is worth mentioning that the new method works for any $r_k \in [q^k/\sqrt{2}, q^k)$ (instead of (42)), i.e., the circles can be chosen as large as possible so that each circle $\partial D_{k,j}$ encloses the square $S_{k,j}$, and that these circles are disjoint. Numerical experiments (not presented in this paper) show that the new method produces a decreasing sequence of approximate values for $\text{cap}(D_k)$ if we choose, for example, $r_k = 1.25q^k/\sqrt{2}$. Note that the proof of Theorem 4.1 can be adapted to see that $\text{cap}(F) = \lim_{k \rightarrow \infty} \text{cap}(D_k)$ also holds for these larger radii.

Example 4.4 (Generalized Cantor dust). We consider now the numerical approximation of $\text{cap}(F)$ for general $q \in (0, 0.5)$. For the limiting cases $F = \{0, 1, 1 + i, i\}$ (corresponding to $q = 0$) and $F = [0, 1] \times [0, 1]$ (corresponding to $q = 0.5$), the capacities are

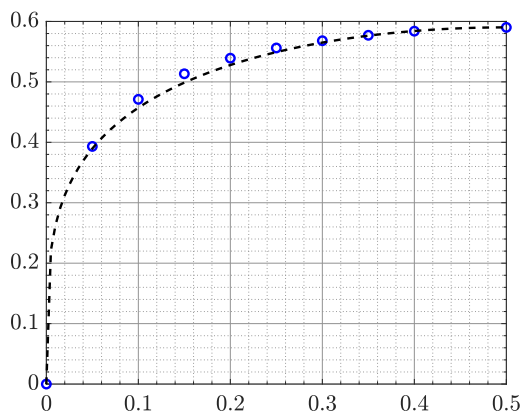
$$\text{cap}(F) = 0 \quad \text{and} \quad \text{cap}(F) = \frac{\Gamma(1/4)^2}{4\pi\sqrt{\pi}} \approx 0.590170299508048,$$

respectively; see [14, Table 1]. The new method can be used for $q < \sqrt{2} - 1$, so that the disks $D_{k,j}$ with the radius r_k given by (42) are disjoint. Here we use the method to approximate the value of $\text{cap}(F)$ for $q = 1/20, 2/20, \dots, 8/20$.

Similar to Example 4.3, the sequences of the computed approximations of $\text{cap}(D_k)$ are not necessarily decreasing. For this example, the method generates a decreasing sequence of approximate values for $q = 1/20, \dots, 5/20$, and an increasing sequence for $q = 6/20, 7/20, 8/20$. Then, using the approach described in Example 4.3, the obtained approximate values are extrapolated to obtain approximations for $\text{cap}(F)$, which are stated in Table 6.

Table 6: The computed approximations of $\text{cap}(F)$; see Example 4.4.

q	$\text{cap}(F)$
1/20	0.393193419290132
2/20	0.471075541819326
3/20	0.513383693856075
4/20	0.539195036874426
5/20	0.55611125682008
6/20	0.568071614755641
7/20	0.577089193675801
8/20	0.583884621972929

Figure 13: The computed logarithmic capacity $\text{cap}(F)$ (blue circles) and the function f in (49) (dashed).

Similarly to the generalized Cantor sets, it would be of interest to closely approximate the values of $\text{cap}(F)$ with a function of $q \in [0, 0.5]$. After some attempts we came up with

$$f(q) = \sqrt{2} \frac{\Gamma(1/4)^2}{4\pi\sqrt{\pi}} (q(1-q))^{1/4}, \quad (49)$$

which is shown in Figure 13. It is another open question to determine whether there is an exact analytic relation between the logarithmic capacities of the generalized Cantor set and generalized Cantor dust. The only relation we are aware of is $\text{cap}(F) \geq 2\text{cap}(E)$; see [24, p. 1516].

5 Concluding remarks

In this paper we have applied the CSM to the computation of the logarithmic capacity of compact sets consisting of very many “small” components. This application allows to use just a single charge point for each component, which leads to a significantly more efficient computational method in comparison with methods that use discretizations of the boundaries of the different components. We have obtained an additional speedup of the method by exploiting the structure of the system matrices, and by using a problem-adapted preconditioner for the linear algebraic systems. In the numerical examples we have seen that for the same number of components, the new method is faster by a factor of 100 (sometimes even 1000) than our previous BIE method [14], while maintaining the same high level of accuracy. We have applied the method to generalized Cantor sets and the Cantor dust. We are not aware of any other computed approximations of the logarithmic capacity of the Cantor dust for $q \neq 1/3$ in the literature.

References

- [1] K. AMANO, *A charge simulation method for numerical conformal mapping onto circular and radial slit domains*, SIAM J. Sci. Comput., 19 (1998), pp. 1169–1187.
- [2] K. AMANO AND D. OKANO, *A circular and radial slit mapping of unbounded multiply connected domains*, JSIAM Lett., 2 (2010), pp. 53–56.
- [3] M. A. AUGUSTIN, *A Method of Fundamental Solutions in Poroelasticity to Model the Stress Field in Geothermal Reservoirs*, Lecture Notes in Geosystems Mathematics and Computing, Birkhäuser Basel, 1995.
- [4] P. BADDOO AND L. N. TREFETHEN, *Log-lightning computation of capacity and Green’s function*, Maple Trans., 1 (2021), pp. 1–13. Article 14124.
- [5] W. DIJKSTRA AND M. E. HOCHSTENBACH, *Numerical approximation of the logarithmic capacity*, CASA report, 0809 (2009).
- [6] H. FASSBENDER AND K. D. IKRAMOV, *Computing matrix-vector products with centrosymmetric and centrohermitian matrices*, Linear Algebra Appl., 364 (2003), pp. 235–241.
- [7] J. B. GARNETT AND D. E. MARSHALL, *Harmonic measure*, vol. 2 of New Mathematical Monographs, Cambridge University Press, Cambridge, 2005.
- [8] L. GREENGARD AND Z. GIMBUTAS, *FMMLIB2D: A MATLAB toolbox for fast multipole method in two dimensions*, version 1.2. ed., 2012. <http://www.cims.nyu.edu/cmcl/fmm2dlib/fmm2dlib.html>. Accessed 1 Jan 2018.
- [9] L. GREENGARD AND V. ROKHLIN, *A fast algorithm for particle simulations*, J. Comput. Phys., 73 (1987), pp. 325–348.
- [10] J. HELSING AND E. WADBRO, *Laplace’s equation and the Dirichlet-Neumann map: a new mode for Mikhlin’s method*, J. Comput. Phys., 202 (2005), pp. 391–410.
- [11] M. R. HESTENES AND E. STIEFEL, *Methods of conjugate gradients for solving linear systems*, J. Research Nat. Bur. Standards, 49 (1952), pp. 409–436.
- [12] E. KALMOUN AND M. NASSER, *Harmonic image inpainting using the charge simulation method*, Pattern Anal Applic, 25 (2022), pp. 795–806.
- [13] H. KRÜGER AND B. SIMON, *Cantor polynomials and some related classes of OPRL*, J. Approx. Theory, 191 (2015), pp. 71–93.
- [14] J. LIESEN, O. SÈTE, AND M. M. S. NASSER, *Fast and accurate computation of the logarithmic capacity of compact sets*, Comput. Methods Funct. Theory, 17 (2017), pp. 689–713.
- [15] J. LIESEN AND Z. STRAKOŠ, *Krylov subspace methods. Principles and analysis*, Numerical Mathematics and Scientific Computation, Oxford University Press, Oxford, 2013.
- [16] G. MEURANT AND Z. STRAKOŠ, *The Lanczos and conjugate gradient algorithms in finite precision arithmetic*, Acta Numer., 15 (2006), pp. 471–542.
- [17] C. D. MINDA, *Capacity estimates for planar cantor-like sets*, Can. J. Math., 26 (1974), pp. 1169–1172.

- [18] M. M. S. NASSER, J. LIESEN, AND O. SÈTE, *Numerical computation of the conformal map onto lemniscatic domains*, Comput. Methods Funct. Theory, 16 (2016), pp. 609–635.
- [19] H. OGATA, D. OKANO, M. SUGIHARA, AND K. AMANO, *Unique solvability of the linear system appearing in the invariant scheme of the charge simulation method*, Japan J. Indust. Appl. Math., 20 (2003), pp. 17–35.
- [20] D. OKANO, H. OGATA, AND K. AMANO, *A method of numerical conformal mapping of curved slit domains by the charge simulation method*, in Proceedings of the International Conference on Recent Advances in Computational Mathematics (ICRACM 2001) (Matsuyama), vol. 152, 2003, pp. 441–450.
- [21] C. C. PAIGE AND M. A. SAUNDERS, *Solutions of sparse indefinite systems of linear equations*, SIAM J. Numer. Anal., 12 (1975), pp. 617–629.
- [22] T. RANSFORD, *Potential theory in the complex plane*, vol. 28 of London Mathematical Society Student Texts, Cambridge University Press, Cambridge, 1995.
- [23] ———, *Computation of logarithmic capacity*, Comput. Methods Funct. Theory, 10 (2010), pp. 555–578.
- [24] T. RANSFORD AND J. ROSTAND, *Computation of capacity*, Math. Comp., 76 (2007), pp. 1499–1520.
- [25] J. ROSTAND, *Computing logarithmic capacity with linear programming*, Experiment. Math., 6 (1997), pp. 221–238.
- [26] Y. SAAD AND M. H. SCHULTZ, *GMRES: a generalized minimal residual algorithm for solving nonsymmetric linear systems*, SIAM J. Sci. Statist. Comput., 7 (1986), pp. 856–869.
- [27] O. SÈTE AND J. LIESEN, *On conformal maps from multiply connected domains onto lemniscatic domains*, Electron. Trans. Numer. Anal., 45 (2016), pp. 1–15.
- [28] G. SZEGÖ, *Bemerkungen zu einer Arbeit von Herrn M. Fekete: Über die Verteilung der Wurzeln bei gewissen algebraischen Gleichungen mit ganzzahligen Koeffizienten*, Math. Z., 21 (1924), pp. 203–208.
- [29] J. L. WALSH, *On the conformal mapping of multiply connected regions*, Trans. Amer. Math. Soc., 82 (1956), pp. 128–146.
- [30] H. WANG AND Q.-H. QIN, *Methods of Fundamental Solutions in Solid Mechanics*, Elsevier, 2020.
- [31] E. WEGERT, *Visual complex functions*, Birkhäuser/Springer Basel AG, Basel, 2012.